Inertia Identification for the Speed Observer of the Low Speed Control of Induction Machines

Nam-Joon Kim, *Student Member, IEEE*, Hee-Sung Moon, *Student Member, IEEE*, and Dong-Seok Hyun, *Senior Member, IEEE*

***Abstract*—This paper presents a control method for induction machines in a low speed range with an instantaneous speed observer and inertia identification. When the low resolution incremental-type encoder is used for the speed detection, we only obtain the average speed in the interval of the encoder pulses, and it usually makes the speed controller unstable at the very low speed range. This paper, therefore, proposes a low speed control method with a speed observer which is implemented by the disturbance observer using a low percision shaft encoder. Furthermore, to improve the performance of the speed controller, we will perform the identification of the inertia which is estimated by the periodic test signal. We will show that this proposed method is superior to the conventional method by simulation and experiment results.**

***Index Terms*—Low speed control, instantaneous speed estimation, inertia estimation, inertia identification, disturbance torque observer.**

I. Introduction

RECENTLY, there has been a remarkably high development of the digital signal processor, which is able to process accurate computation within a short sampling period. We have widely applied this to a servo system that demands a high degree of flexibility in the control of speed and torque among various industrial control system areas.

For this type of control system, it is very important that the suitable application of the speed sensor for the accurate speed information. Considering the cost and the performance of the control system, we usually select the low precision incremental encoder. However, this type of encoder detects only the average speed in the interval of the pulses, and this average speed information has the detection dead time which is increased under the low speed regions. In these circumstances, it is a matter for deep reflection that the detection dead time has an influence on the performance of the overall speed control system. To improve the performance of the speed control system which has been degraded by the detection dead time, there are many papers proposing instantaneous speed control by the application of a state observer, especially a disturbance observer [1]–[7].

This state observer is easily implemented in the speed control system because it has a simple structure and the robustness against the variation of the inertia. Even though the inertia of the machine is unknown or initially incorrect, it is generally true that the speed control system is stabilized by the its feedback gain. In real system implementation, the time constant of the speed observer has to be small. However, it is difficult to implement the time constant, which must be as small as possible, because of the backlash or the noise in mechanical systems. Consequently, the overall speed control system must be controlled by the identification of the inertia to be obtained by the inertia estimation [8]–[10].

In this paper, to solve the speed sensing problem under low speed conditions, the instantaneous speed observer is implemented by the disturbance torque estimator. Also, to improve the degraded performance of the speed controller according to the unknown or varied inertia of the machine, the inertia identification is performed with the estimated inertia to be obtained by the periodic test signal in the speed controller. We will show that the proposed method is superior to the conventional speed control in simulations and experiments. The experiments are performed with the digital signal processor (*TMS320C31*) for the inertia identification as well as the speed control at the low speed range.

II. Speed Sensing Characteristics

Generally, the speed sensing of the machine is founded on the pulses of the encoder which is a speed detector. The mechanical position variation of the machine is represented by the calculation of the encoder pulse number. In order to obtain the speed information, it is performed that the differentiation of the position information in each sampling period, and the speed information from this sequence is the average speed during a sampling period.

Fig. 1 shows the relationship between the speed sampling interval and the encoder pulses. The speed information is obtained by calculating the pulse number (M) within a sampling period. It is general that the resolution of the encoder is established as highly as possible in the middle/high speed range. In spite of the high precision encoder, however, a pulse interval (T_p) becomes longer than the speed sampling interval (T_s) under very low speed regions. Occasionally, only one pulse comes in during several sampling intervals. In the middle

Paper IPCSD 96-37, approved by the Industrial Drives Committee and the Industrial Automation and Control Committee of the IEEE Industry Applications Society for presentation at the 1995 Industry Applications Society Annual Meeting, Lake Buena Vista, FL, October 9–13. Manuscript released for publication May 23, 1996.

N.-J. Kim is with the Department of Electrical Engineering, Daejin University, Pocheon-eup, Pocheon-kun, Kyunggi-do 487-800, Korea.

H.-S. Moon and D.-S. Hyun are with the Department of Electrical Engineering, Hanyang University, 17, Hangdang-dong, Seongdong-Ku, Seoul 133-791, Korea.

Publisher Item Identifier S 0093-9994(96)07069-7.

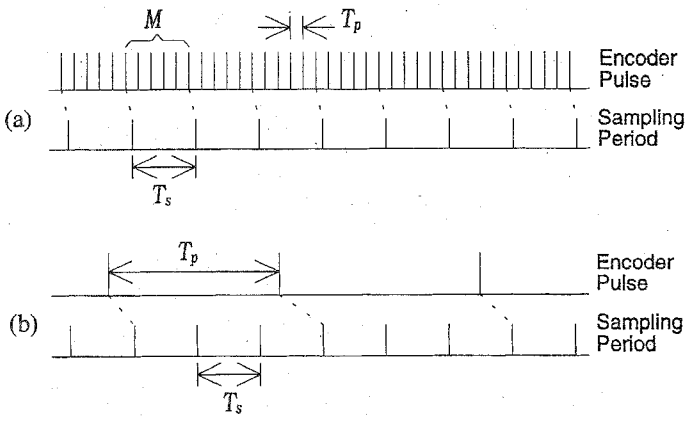

Fig. 1. Relation between encoder pulse and sampling period. (a) Middle/high speed range. (b) Low speed range.

or high speed range, we can easily obtain highly accurate speed information at every sampling time.

On the other hand, at the low speed, the speed sensing is performed by an incoming instant of the encoder pulse. This means that the speed sensing information is delayed in some measure. On this occasion, the maximum detection dead time of the middle/high and low speed range can be expressed as (1) and (2), respectively,

$$T_d = \frac{T_s}{2} + T_p \tag{1}$$

$$T_d = \tfrac{1}{2}T_p + T_s. \tag{2}$$

As above, if the encoder pulse is longer than the sampling interval, that is, at the low speed range, the detection dead time will be abruptly expanded.

From now on, we can examine the effect of the speed detection deadtime on the stability of the speed feedback controller. The open-loop speed transfer function, without regard for the inner control loop delay of the speed controller, is shown as (3). In (3), f_s is the response frequency of the speed controller and s is the Laplacian operator. In order for the controller to be stable, in the case where the operating frequency f is equal to f_s, the phase delay should be smaller than $\pi/2$ rad.

$$\frac{\omega_m(s)}{\omega_m^*(s)} = \frac{2\pi \cdot f_s}{s}\exp(-s \cdot T_d) \tag{3}$$

$$2\pi \cdot f_s T_d \le \frac{\pi}{2} \tag{4}$$

where ω_m^* is the speed reference.

In view of rotating N r/m with the P ppr precision encoder for the speed sensing, the interval of encoder pulse is shown.

$$T_p = \frac{60}{N \cdot P}. \tag{5}$$

In case that the encoder pulse is longer than the sampling period, that is, in the very low speed regions, a controllable speed of the machine is calculated as stably as possible by (2), (4), and (5) as (6):

$$N = \frac{120 f_s}{(1 - 4 f_s \cdot T_s)P}. \tag{6}$$

For example, in cases that 1) the required speed response characteristics is 50 Hz, 2) the speed information is obtained by the encoder with 4096 ppr resolution, 3) the speed sampling time is 1 ms, we will determine that the controllable speed as stably as possible is nearly 1.8 r/m.

III. Instantaneous Speed and Inertia Estimation

A. The Model of Control System

The developed torque of the induction machine with the vector control system is simplified such as a dc machine model. The block diagram of this simplified machine model combined with an encoder is represented in Fig. 2.

In Fig. 2, the discretizing state equation of the plant is described as (7). In (7), τ_e is the developed torque of the machine, $\overline{\omega}_m$ is the average speed, τ_d is the disturbance torque, and J is the equivalent inertia moment. We expect that the variation of the disturbance torque is slower than the unit sampling time, and the disturbance torque is expressed as (8). We can represent the state equation with respect to the following relationships:

$$\overline{\omega}_m(i+1) = \overline{\omega}_m(i) + \frac{T_s}{J}\{\tau_e(i) - \tau_d(i)\} \tag{7}$$

$$\tau_d(i+1) = \tau_d(i) \tag{8}$$

$$X(i+1) = AX(i) + BU(i) \tag{9}$$

$$Y(i) = CX(i) \tag{10}$$

where

$$U(i) = \tau_e(i), \quad X(i) = \begin{bmatrix} \omega_m(i) \\ \tau_d(i) \end{bmatrix}, \quad Y(i) = \overline{\omega}_m(i)$$

$$A = \begin{bmatrix} 1 & -\dfrac{T_s}{J} \\ 0 & 1 \end{bmatrix} = \begin{bmatrix} a_{11} & a_{12} \\ a_{21} & a_{22} \end{bmatrix},$$

$$B = \begin{bmatrix} \dfrac{T_s}{J} \\ 0 \end{bmatrix} = \begin{bmatrix} b_1 \\ b_2 \end{bmatrix}, \quad C = [1 \quad 0]$$

B. Disturbance Torque Observer

Equations (9) and (10) are an observable system, and we can compose the state observer for estimating τ_d as (11) and (12). In discretizing time domains, the reduced-order observer is applied to (13) and (14) from (11) and (12), and then the simplified block diagram of the disturbance observer is shown in Fig. 3.

$$Z(i+1) = \hat{A}Z(i) + \hat{K}Y(i) + \hat{B}U(i) \tag{11}$$

$$\hat{X}(i) = \hat{C}Z(i) + \hat{D}Y(i) \tag{12}$$

where

$$\hat{A} = 1 - L \cdot a_{12}, \quad \hat{K} = L - L^2 \cdot a_{12} - L \cdot a_{11},$$

$$\hat{B} = b_2 - L \cdot b_1$$

$$\hat{C} = \begin{bmatrix} 0 \\ 1 \end{bmatrix}, \quad \hat{D} = \begin{bmatrix} 0 \\ L \end{bmatrix}$$

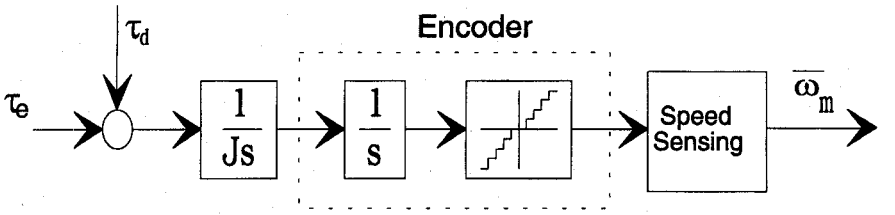

Fig. 2. Block diagram of plant.

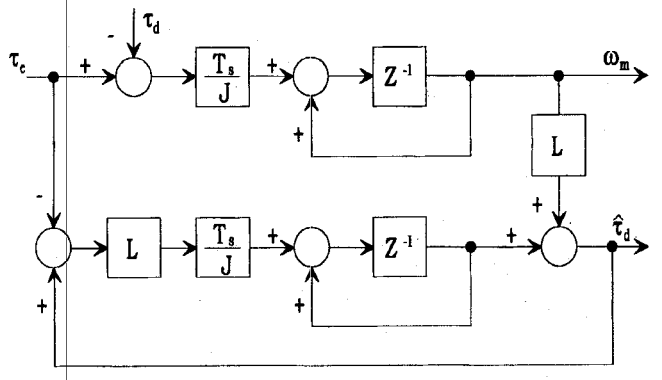

Fig. 3. Simplified block diagram composed by reduced-order observer.

$$Z(i+1) = Z(i) + L \cdot \frac{T_s}{J}\{\hat{\tau}_d(i) - \tau_e(i)\} \tag{13}$$

$$\hat{\tau}_d(i) = Z(i) + L \cdot \overline{\omega}_m(i) \tag{14}$$

where Z is internal variable and L is observer gain.

In order to inspect the stability of the observer, the estimated error of the disturbance torque is constructed as (15), and it is represented as (16) by (13), (14). From (16), the condition of the convergence of the observer is determined by the eigenvalue of $\hat{A}$, that is, the pole placement of the observer is a function of the gain L. Therefore, the convergence time is decided on a proper selection of the gain L:

$$e(i) = \hat{\tau}(i) - \tau_d(i) \tag{15}$$

$$e(i+1) = \hat{A} \cdot e(i) \tag{16}$$

$$|\hat{A}| = |1 - L \cdot a_{12}| < 1. \tag{17}$$

C. Calculation of Instantaneous Speed

It is generally true that the machine speed information is substantially provided by the encoder pulse. Its speed information by the calculation within a sampling period is merely the average speed. Therefore, this speed information includes the dead time, and it increases more and more under low speed conditions.

The relationship of the encoder pulses and the sampling period of the controller at a very low speed range is shown in Fig. 4.

In Fig. 4, the speed information which is sensed at the ith speed sampling point is not the real speed at this point; it is just the average speed within the $T_p(j)$ interval. We consider that the imaginary sampling point k is the middle point of $T_p(j)$, and then the ith sampling speed information is the instantaneous speed of the imaginary sampling point k. Therefore, the instantaneous speed of the ith sampling point

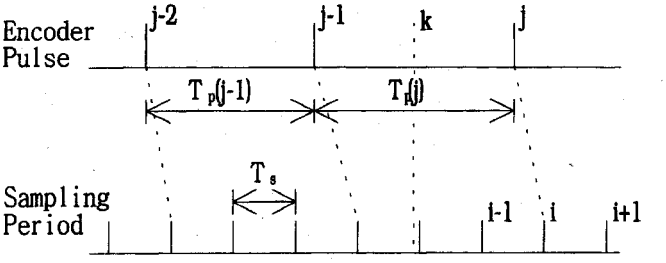

Fig. 4. Encoder pulse and sampling period at low speed range.

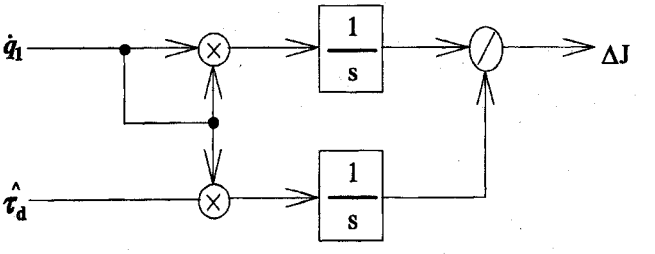

Fig. 5. Block diagram of the inertia variation estimation.

is delayed during $T_p(j)/2 + T_s$ with the maximum condition. Furthermore, the instantaneous speed of the ith sampling point is calculated from the acceleration torque; it can be calculated from the difference between the estimated disturbance torque and the torque applied to the machine during $T_p(j)/2$ on the basis of the speed information at the imaginary sampling point k. By the same calculation, we acquire that the instantaneous speed information at the $i+1, i+2, \cdots, i_n-$th sampling points; we cannot obtain even the average speed at these points. For the calculation of the speed information, we adopt the linearization of the current command of the torque component with regard to the real system application:

$$\hat{\omega}_m(i) = \overline{\omega}(i) + \frac{1}{J}\int_{t-T_p/2}^{t} \{\tau_e(i) - \hat{\tau}_d(i)\}\, dt \tag{18}$$

$$\hat{\omega}_m(i+1) = \hat{\omega}_m(i) + \frac{T_s}{J}\sum_{l=1}^{n}\{\tau_e(i+l-1) - \hat{\tau}_d(i+l-1)\}. \tag{19}$$

D. Inertia Identification

Until now, the instantaneous speed controller at the low speed region has the nominal inertia value (J_n) of the induction machine model; it is the same as the equivalent value (J). It is generally true that the stability of the speed controller is obtained by the controller gain in spite of the incorrect inertia information. In the real system implementation, the time

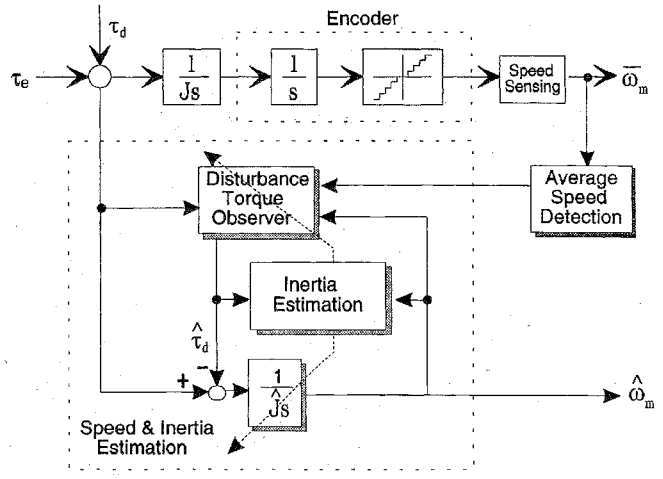

Fig. 6. Speed control system with inertia identification.

TABLE I
PARAMETERS OF INDUCTION MACHINE

Rated Power	3[Hp]	R_r	1.28[Ω]
Rated Voltage	220[V]	L_s	108[mH]
Rated Current	8.6[A]	L_r	108[mH]
No. of Poles	4	L_m	105[mH]
R_s	1.26[Ω]	J	0.075[kg·m^2]

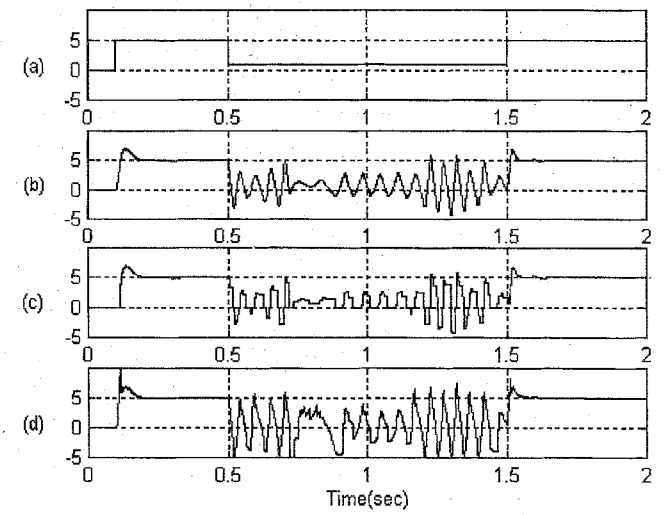

Fig. 7. Speed characteristics with conventional speed sensing (Simulation). (a) Speed reference. (5 r/m/div.) (b) Real speed. (5 r/m/div.) (c) Calculated speed. (5 r/m/div.) (d) Estimated speed. (5 r/m/div.).

constant of the observer should be small; however, it is difficult to realize the need for a small time constant because of the backlash or noise in a mechanical system. Consequently, the overall speed control system of the induction machine must be controlled by the identification of the inertia to be obtained by the estimation.

In this paper, we can estimate the inertia of the machine according to the relationship of the mathematical orthogonality of the internal state variables in the disturbance observer,

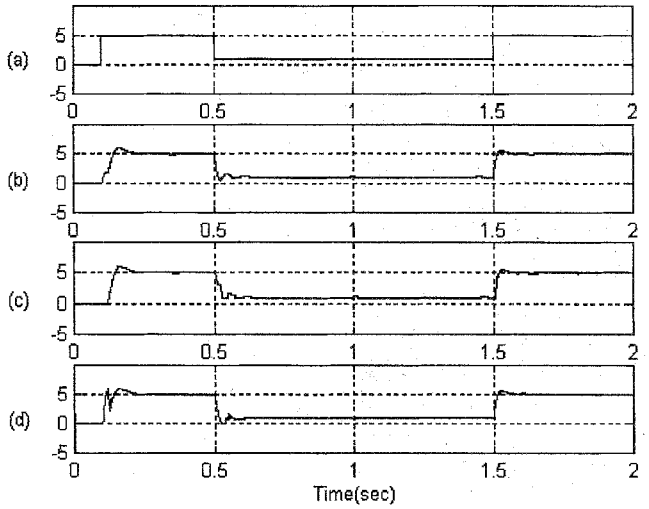

Fig. 8. Speed characteristics with proposed speed sensing (Simulation). (a) Speed reference. (5 r/m/div). (b) Real speed (5 r/m/div). (c) Calculated speed. (5 r/m/div). (d) Estimated speed. (5 r/m/div).

which is used for the instantaneous speed estimation. For the purpose of the estimation, we imposed the periodic speed reference in order to acquire the convergence of the estimated inertia, and we considered that the various servo system had a similar speed reference. In this estimation, we use the disturbance torque observer and modify to internal state variables as (22) and (23):

$$\frac{dz(t)}{dt} = \lambda \cdot z(t) + \lambda \cdot J_n \cdot \hat{\omega}_m(t) + \tau_e(t) \tag{20}$$

$$\hat{\tau}_d(t) = -\lambda \cdot z(t) + \lambda \cdot J_n \cdot \hat{\omega}_m(t) = J_n \cdot \dot{q}_1(t) - q_0(t) \tag{21}$$

$$\frac{dq_0(t)}{dt} = -\lambda \cdot q_0(t) + \lambda \cdot \tau_e(t) \tag{22}$$

$$\frac{dq_1(t)}{dt} = -\lambda \cdot q_1(t) + \lambda \cdot \hat{\omega}_m(t) \tag{23}$$

where λ is observer pole, q_0 and q_1 are the internal state variables.

Inertia variation ΔJ is caused by a load change or an estimation error of the inertia, and it is expressed as (24). From (24), the differential equation of estimated disturbance torque is derived as (25), and it is represented by internal state variables q_1, q_2 as (26):

$$\Delta J = \hat{J} - J_n \tag{24}$$

$$\frac{d\hat{\tau}_d(t)}{dt} = -\lambda \cdot \hat{\tau}_d(t) - \lambda(\Delta J \cdot \frac{d\hat{\omega}_m(t)}{dt} + D \cdot \hat{\omega}_m(t) - T_c) \tag{25}$$

$$\hat{\tau}_d(t) = -\Delta J \cdot \dot{q}_1(t) - D \cdot q_1(t) + T_c \cdot q_2(t) \tag{26}$$

$$\frac{dq_2(t)}{dt} = -\lambda \cdot q_2(t) + \lambda \tag{27}$$

where D is the viscous and T_c is the constant disturbance torque.

In the system driven by a servo velocity controller, we can consider that the speed reference is a periodic. Therefore, the speed reference can be expressed according to the speed reference period T as (28). Furthermore, internal state variables

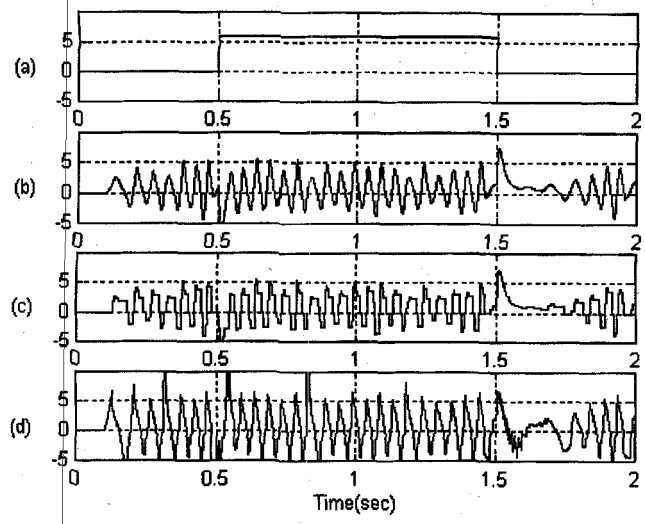

Fig. 9. Load characteristics with conventional speed sensing (Simulation). (a) Load torque. (5 N·m/div). (b) Real speed (5 r/m/div). (c) Calculated speed (5 r/m/div.) (d) Estimated speed (5 r/m/div).

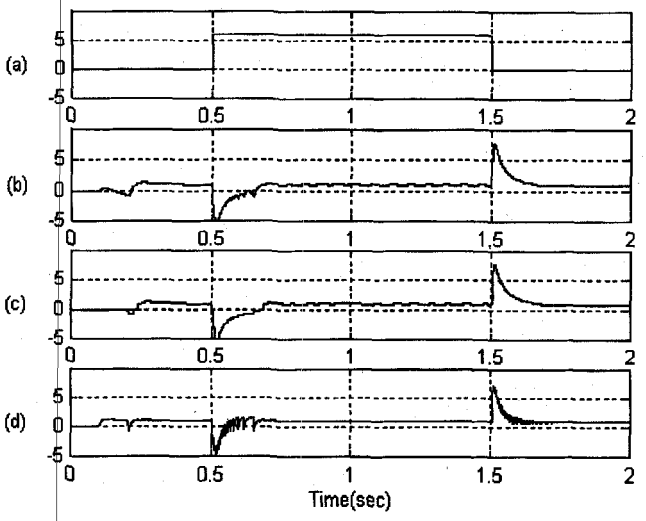

Fig. 10. Load characteristics with proposed speed sensing (Simulation). (a) Load torque. (5 N·m/div.) (b) Real speed. (5 r/m/div.) (c) Calculated speed. (5 r/m/div.) (d) Estimated speed. (5 r/m/div.).

are represented such as (29)-(31), respectively,

$$\lim_{t\to\infty}[\omega_m(t)-\omega_m(t-T)]=0. \tag{28}$$

$$\lim_{t\to\infty}[q_1(t)-q_1(t-T)]=0. \tag{29}$$

$$\lim_{t\to\infty} q_2(t)=1. \tag{30}$$

$$\lim_{t\to\infty}\dot{q}_2(t)=0. \tag{31}$$

From now on, the inner product of the arbitrary input signals ψ_a and ψ_b is defined as (32). According to the inner product of the internal state variables $q_1, \dot{q}_1$ and $q_2, \dot{q}_1$, we can obtain the relationship, respectively, as

$$[\psi_a,\psi_b]=\int_{(k-1)T}^{kT}\psi_a(t)\cdot\psi_b(t)dt \tag{32}$$

$$\lim_{k\to\infty}\int_{(k-1)T}^{kT} q_1(t)\cdot\dot{q}_1(t)dt=0 \tag{33}$$

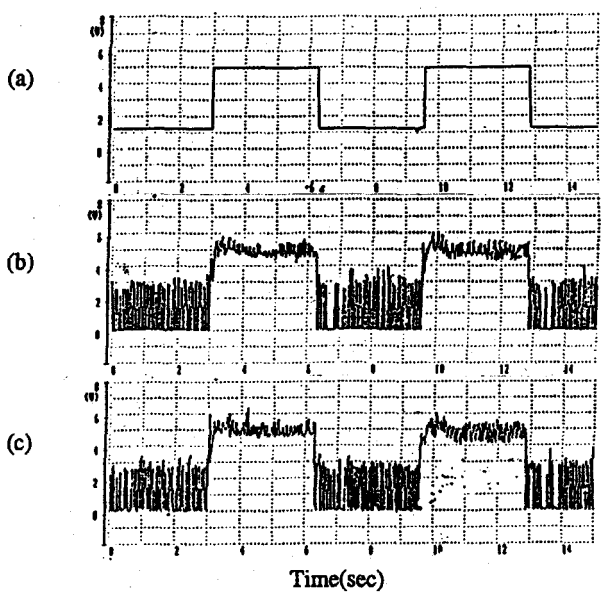

Fig. 11. Speed characteristics with conventional speed sensing (Experiment). (a) Speed reference. (1 r/m/Div.) (b) Calculated Speed. (1 r/m/Div.) (c) Estimated speed. (1 r/m/Div.).

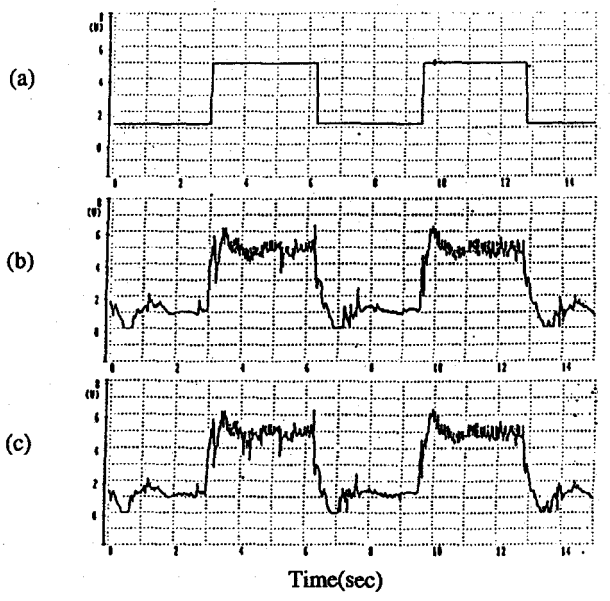

Fig. 12. Speed characteristics with proposed speed sensing (Experiment). (a) Speed reference. (1 r/m/Div.) (b) Calculated Speed. (1 r/m/Div.) (c) Estimated speed. (1 r/m/Div.).

$$\lim_{k\to\infty}\int_{(k-1)T}^{kT} q_2(t)\cdot\dot{q}_1(t)dt=0. \tag{34}$$

In order to estimate the inertia variation, we can modify the above relations as (35)–(37) where $\Delta J(k)$ is the estimated inertia variation during kT, $\hat{J}(k)$ is the estimated value of the inertia. Fig. 5 is the block diagram of the inertia variation estimation and Fig. 6 is the overall speed control scheme with the inertia identification and the speed estimation:

$$\lim_{k\to\infty}\int_{(k-1)T}^{kT}\hat{\tau}_d(t)\cdot\dot{q}_1(t)dt=-\Delta J\cdot\lim_{k\to\infty}\int_{(k-1)T}^{kT}\dot{q}_1(t)^2dt \tag{35}$$

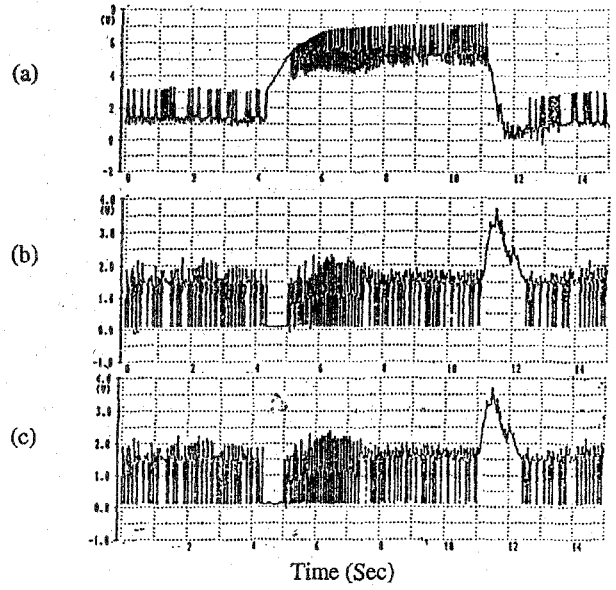

Fig. 13. Load characteristics with conventional speed sensing (Experiment). (a) Torque component current. (1 A/div.) (b) Calculated speed. (1 r/m/div.) (c) Estimated speed. (1 r/m/div.).

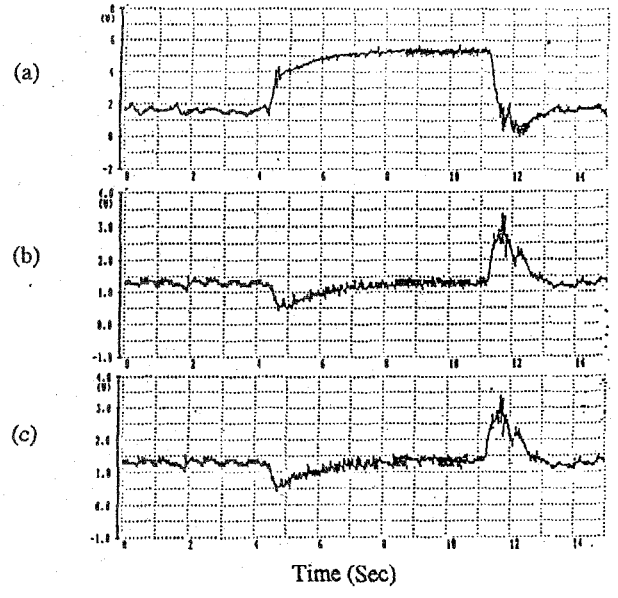

Fig. 14. Load characteristics with proposed speed sensing (Experiment). (a) Torque component current. (1 A/div.) (b) Calculated speed. (1 r/m/div.) (c) Estimated speed. (1 r/m/div.).

$$\Delta J(k) = -\lim_{k\to\infty} \frac{\int_{(k-1)T}^{kT} \hat{\tau}_d(t)\cdot \dot{q}_1(t)dt}{\int_{k-1)T}^{kT} \dot{q}_1(t)^2 dt}, \qquad k = 1, 2, \cdots \tag{36}$$

$$\hat{J}(k) = J_n + \Delta J(k). \tag{37}$$

IV. Simulation and Experiment

We performed the simulation and experiment about the proposed algorithm for the induction machine with Table I. To detect the speed information, we used the incremental encoder with 4096 ppr resolution; it naturally has the resolution of 1024 ppr, but we adjusted the resolution to 4096[ppr] by using a multiplier. The speed and current control sampling times are 2 ms and 100 μs, respectively. The gain of the disturbance torque observer is -7.5. The overall speed control system is implemented in the DSP (*Digital Signal Processor*: *TMS320C31*) for the real-time control of the proposed algorithm and the space vector PWM control.

The sequence of the simulation and experiment is as follows. First, the instantaneous speed is estimated by the disturbance torque observer. Second, a comparison is made between the speed characteristics with the conventional PI controller and the speed characteristics with the instantaneous speed estimation. Third, a comparison is also made between the load characteristics with the PI controller and the load characteristics with the speed estimation. Fourth, considering

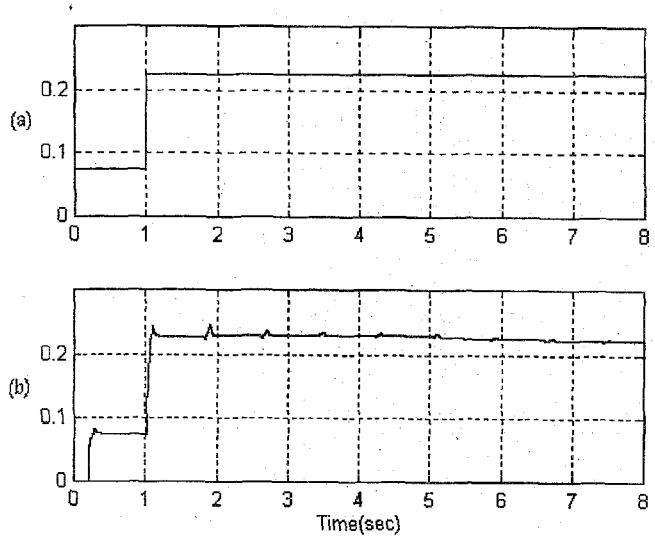

Fig. 15. Inertia estimation according to the periodic speed reference with the gain $L = -15.0$ (Simulation). (a) Inertia variation $J_n \rightarrow 3J_n$. (0.1 kg·m^2/div). (b) Estimated inertia. (0.1 kg·m^2/div).

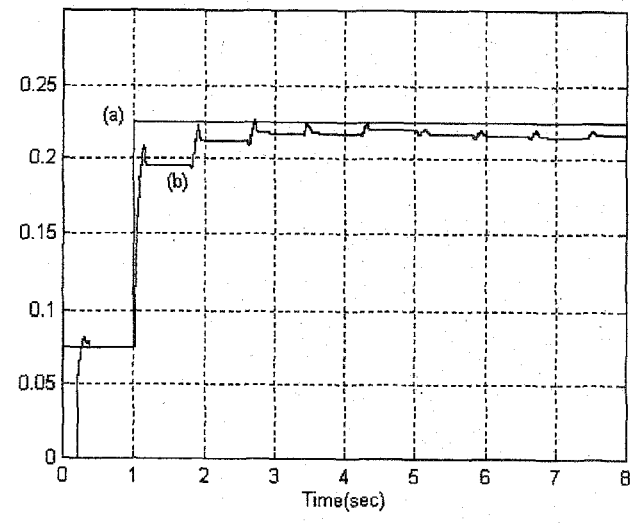

Fig. 16. Inertia estimation according to the periodic speed reference with the gain $L = -7.5$ (Simulation). (a) Inertia variation $J_n \rightarrow 3J_n$. (0.05 kg·m^2/div). (b) Estimated inertia. (0.05 kg·m^2/div).

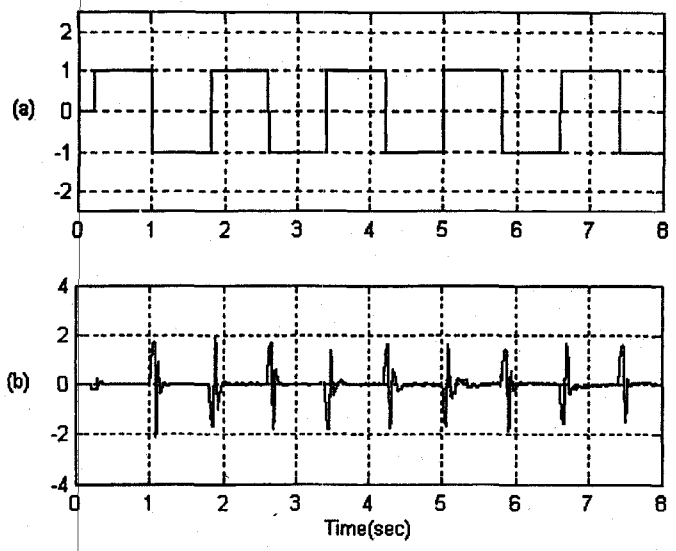

Fig. 17. Periodic speed reference during inertia estimation with the gain $L = -15.0$ (Simulation). (a) Speed reference. (1 r/m/div.) (b) Estimated disturbance torque (2 N·m/div.).

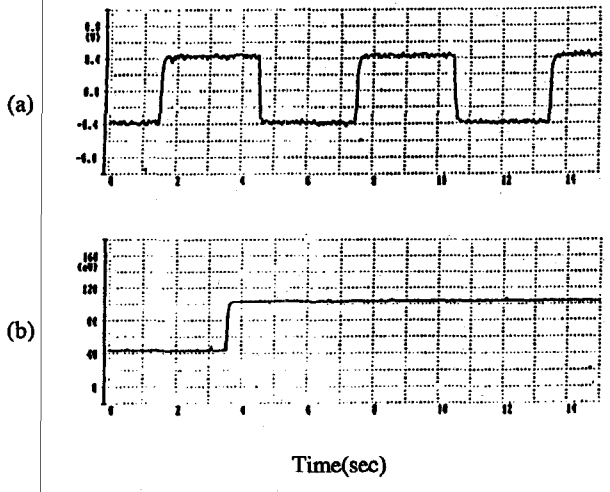

Fig. 18. Inertia estimation according to the periodic speed reference (Experiment). (a) Speed reference. (0.5 r/m/Div.) (b) Estimated inertia.(0.015 kg·m^2/div).

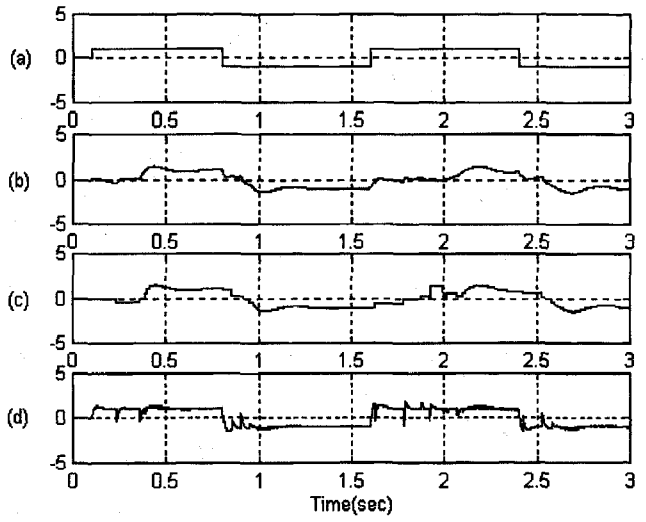

Fig. 19. Speed characteristics without inertia identification (Simulation). (a) Speed reference. (5 r/m/div.) (b) Real speed. (5 r/m/div.) (c) Calculated speed. (5 r/m/Div.) (d) Estimated speed. (5 r/m/div.).

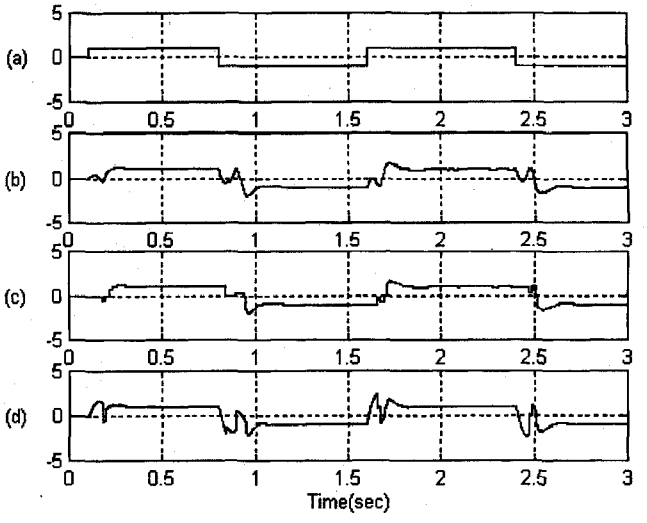

Fig. 20. Speed characteristics with inertia identification (Simulation). (a) Speed reference. (5 r/m/div.) (b) Real speed. (5 r/m/div.) (c) Calculated speed. (5 r/m/div.) (d) Estimated speed. (5 r/m/div.).

the difference between the nominal inertia of the controller and the real inertia of the mechanical system, the estimated result of the proposed algorithm for the inertia is inspected. Fifth, a comparison is made between the speed characteristics without the identification and the speed characteristics with the identification of the estimated inertia.

Fig. 7 is the simulation result of the conventional speed control in case of speed step command variation from 5 r/m to 1 r/m or from 1 to 5 r/m. Fig. 8 is the speed characteristics of the proposed method with the same condition. It has previously been assumed that the conventional PI speed control is limited to about 2 r/m in Section II. On the contrary, we can know that the proposed method is excellent in spite of very low speed range of about 1 r/m from these figures. Figs. 9 and 10 show the load characteristics at the speed reference 1 r/m. It is shown that the proposed speed control is superior to the conventional control under the load variation.

We also applied the conditions of the simulation to the real system. Figs. 11 and 12 are the speed characteristics of the step speed reference, and Figs. 13 and 14 are the load characteristics of the applied load torque variation. The experiment results, like the simulation, show the stable speed and load characteristics of the proposed method.

Figs. 15 and 16 are the inertia estimation results for the inertia identification of the speed control system with the gain $L = -15.0$ and $L = -7.5$, respectively. For the inertia estimation, we used the test signal of the periodic velocity command from forward 1 r/m to reverse 1 r/m or from reverse 1 r/m to forward 1 r/m as Fig. 17. The inertia variation is intentionally imposed from J_n to $3J_n$ at 1 s. In these figures, it is shown that the varied inertia as well as the initial are well established. Also, it is shown that the convergence rate of the inertia estimation is engaged in the observer gain. Furthermore,

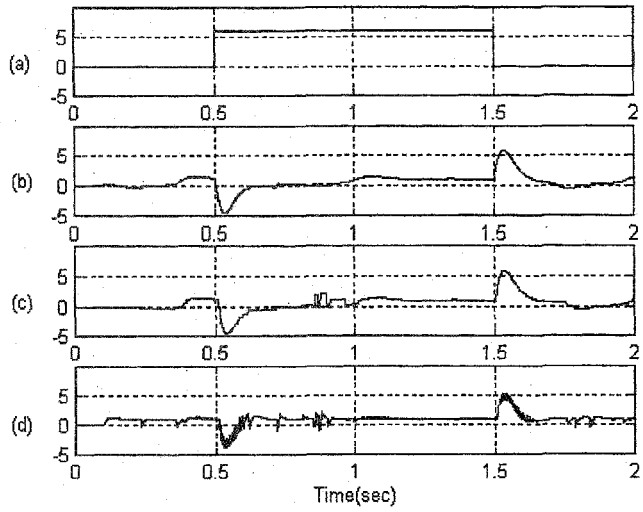

Fig. 21. Load characteristics without inertia identification (Simulation). (a) Load torque. (5 N·m/div.) (b) Real speed. (5 r/m/div.) (c) Calculated speed. (5 r/m/div.) (d) Estimated speed. (5 r/m/Div.).

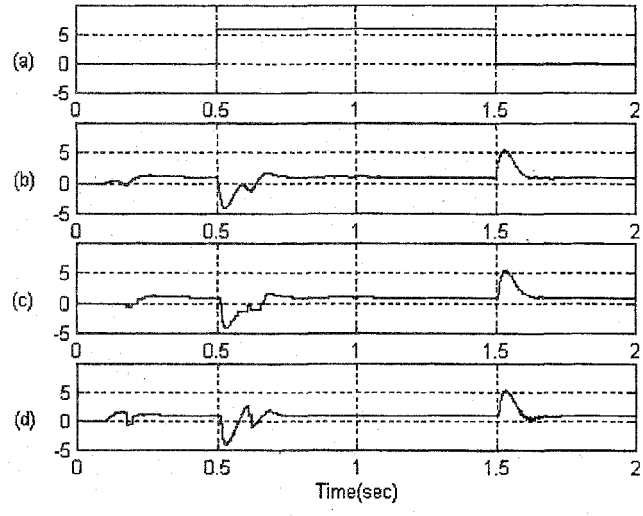

Fig. 22. Load characteristics with inertia identification (Simulation). (a) Load torque. (5 N·m/div.) (b) Real speed. (5 r/m/div.) (c) Calculated speed. (5 r/m/div.) (d) Estimated speed. (5 r/m/div.).

the accuracy of the estimated inertia is concerned with the gain of observer, but it converges to the real system value with small error such as Fig. 15(b) or Fig. 16(b). We can consider that the ripple of the estimated inertia is the estimated error according to the estimated speed error during forward–reverse operation. Fig. 18 is the experimental result of the inertia estimation. The intentional variation of the inertia is caused by the virtual variation that the initial value of the controller is imposed by $0.4J_n$.

Figs. 19 and 20 are the speed characteristics simulation result without and with the inertia identification, respectively. Figs. 21 and 22 are the load characteristics without and with the inertia identification, respectively. Fig. 23 is the experimental result of the speed controller according to the inertia identification. From these figures, we can confirm the improvement of the dynamic characteristics by the identification of the inertia.

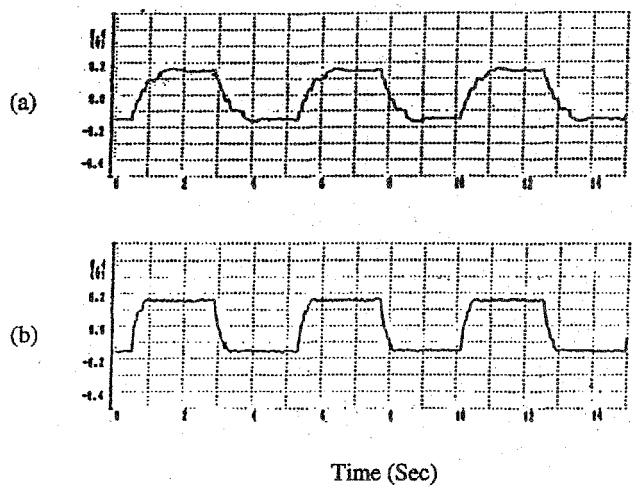

Fig. 23. Speed characteristics of the forward-reverse speed reference (Experiment). (a) without inertia identification. (0.75 r/m/div.) (b) with inertia identification. (0.75 r/m/div.).

V. Conclusion

In this paper, to improve the performance of the low speed control of induction machines, it was introduced that the instantaneous speed control and the inertia estimation be implemented with the disturbance torque observer. Furthermore, it was proposed that the inertia identification by the estimated inertia. The simulation and experiment results showed that the proposed method is better than the conventional one at very low speed range. After this, we consider the study on the on-line inertia estimation and the effect of the instantaneous speed detection according to the inertia variation, respectively.

References

[1] J. P. Rognon, D. Roye, and De Sheng Zhu, "A simple speed observer for digitally controlled motor drives at low speed," in *Conf. Rec. IEEE Ind. Appl. Soc. Ann. Meeting*, 1988, pp. 369–374.

[2] R. D. Lorenz and K. V. Patten, "High resolution velocity estimation for all digital AC Servo Drives," in *Conf. Rec. IEEE Ind. Electron. Soc. Ann. Meeting*, 1988, pp. 363–368.

[3] K. Fujita and K. Sado, "Instantaneous Speed detection with parameter identification for AC servo systems," in *Conf. Rec. IEEE Ind. Electro. Soc. Ann. Meeting*, 1990, pp. 632–638.

[4] Y. Dote, H. Kobayashi, J. Hujikawa, and A. Syitno, "Disturbance observer-based robust and fast speed controller for induction motors," in *Conf. Rec. IEEE Ind. Electron. Soc. Ann. Meeting*, 1990, pp. 653–662.

[5] M. Iwasaki, "Robust speed control of IM with torque feedforward control," in *Conf. Rec. IEEE Ind. Electro. Soc. Ann. Meeting*, 1991, pp. 627–632.

[6] Y. Konno and Y. Hori, "Instantaneous speed observer with improved disturbance rejection performance based on high order dynamics," *Trans. JIEE*, Japan, vol. 112-D, no. 6, pp. 539–544, 1992.

[7] K. Kubo, M. Watanabe, F. Kozawa, and K. Kawasaki, "Disturbance torque compensated speed observer for digital servo drives," in *Conf. Rec. IEEE Ind. Electro. Soc. Ann. Meeting*, 1990, pp. 1182–1187.

[8] Y. Hori, "Robust and Adaptive Control of a Servomotor using Low Precision Shaft Encoder," in *Conf. Rec. IEEE Ind. Electro. Soc. Ann. Meeting*, 1993, pp. 73–78.

[9] I. Awaya, Y. Kato, I. Miyake, and M. Ito, "New motion control with inertia identification function using disturbance observer," in *Conf. Rec. IEEE Ind. Electro. Soc. Ann. Meeting*, 1992, pp. 77–81.

[10] N. J. Kim and D. S. Hyun, "Very low speed control of induction machine by instantaneous speed and inertia estimation," in *Conf. Rec. IEEE Ind. Electro. Soc. Ann. Meeting*, 1994, pp. 21–25.

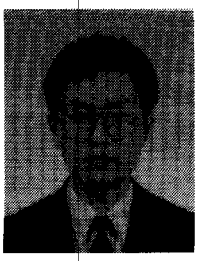

Nam-Joon Kim (S'94) was born in Seoul, Korea, in 1965. He received the B.S. and M.S. degrees in the Department of Electrical Engineering from Hanyang University, Seoul, Korea, in 1988 and 1990, respectively. Currently, he is working toward the Ph.D. degree in the Department of Electrical Engineering at the same university.

Since 1992, he has been with the Department of Electrical Engineering at Daejin University, Kyunggi-do, Korea, where he is engaged as an instructor. His present research interest are in DSP-based ac machine drives, spindle drives and electric vehicles using power electronics.

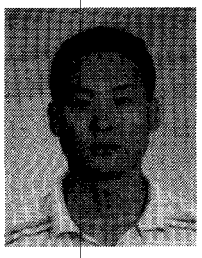

Hee-Sung Moon (S'95) was born in Pusan, Korea, in 1970. He received the B.S. and M.S. degrees from the Department of Electrical Engineering, Hanyang University, Seoul, Korea, in 1994 and 1996, respectively. Currently, he is working toward the Ph.D. degree in the Department of Electrical Engineering at the same university.

He is presently working as a Research Engineer at Technical Research Institute of Hyundai Precision & IND. Co. Ltd., Kyunggi-do, where he is engaged in the department of machine tool engineering. His research interest are in induction machine drives and ac servo machine drives.

Dong-Seok Hyun (S'76–M'86–SM'91) received the B.E. and M.E. degrees in electrical engineering from Hanyang University, Seoul, Korea, in 1973 and 1978, respectively, and the Ph.D. degree in electrical engineering from Seoul National University, Seoul, Korea, in 1986.

From 1976 to 1979, he was the Agency of Defense Development, Korea, as Researcher. He was a Research Associate in the Department of Electrical Engineering at the Univeisity of Toledo during 1984–1985, and a Visiting Professor in Electrical Engineering at Technical University Munich during 1988–1989. Since 1979, he has been at Hanyang University, where he is now a Professor in the Department of Electrical Engineering and Director of the Advanced Institute of Electrical Engineering and Electronics(AIEE). He is the author of more than 80 publications in electric machine design, high power engineering, power electronics motor drives, digital signal processing, tractions and their control system.

Prof. Hyun is a member of the KIEE, the Institution of Electrical Engineers, U.K., and the Power Electronics, Industry Applications, Industrial Electronics, Aerospace and Electronic Systems, Control Systems, and Electron Devices Societies of IEEE.